Mechanics
&
Industry

STANKIN: Innovative manufacturing methods, measurements and materials

REGULAR ARTICLE

D-shell of iron atom of the amorphous FeCr$_{15}$B$_{15}$ alloy effective charge change during the crystallization

Nikolay O. Khmelevsky[1,*], Yuriy V. Funtikov[2], Anatoliy Yu. Aksenenko[1], Olga V. Ilyukhina[2], and Alexander S. Metel[1]

[1] Moscow State University of Technology "STANKIN", 1 Vadkovsky per., Moscow 127055, Russian Federation
[2] Institute for Theoretical and Experimental Physics named by A.I. Alikhanov of National Research Centre "Kurchatov Institute", 25 Bolshaya Cheremushinskaya street, Moscow 117218, Russian Federation

Abstract. An amorphous metal alloy of the FeCrB system was studied during the crystallization by thermal annealing. Such an alloy is a perspective candidate for the role of an intermediate layer in multilayer covering for cutting tools. By the using of the thermoelectric voltage measurement, positron annihilation spectroscopy, and X-ray photoelectron spectroscopy, the conjoint research was performed for the study of the conduction and d-electron band state in the amorphous metallic alloy FeCr$_{15}$B$_{15}$, which intersects each other by the energy. The results of all the studies agree with each other and indicate the change in the effective charge of the d-shell by 1 electron during crystallization.

Keywords: Multilayer covering / metal glass / angular correlation annihilation radiation / valence band / X-ray photoelectron spectroscopy

1 Introduction

Nowadays high magnetic and electric properties of metal glasses are extensively used in technical branches. Power transformers and magnetic heads production based on the amorphous metal alloys and Finemet-type alloys, manufactured on their basis, is growing rapidly every year. At the same time, the development of new ways of for obtaining an amorphous state such as gas-phase deposition [1–4] and selective laser melting [5,6] provides a wider usage of high strength properties of metal glasses. The increase of an amorphous alloys temperature stability leads to a broadening their application range, including the using as a covering for cutting tools [7–9]. Possible using of metal glasses as an intermediate layer in multilayer nanostructured coatings is also actual [10–12]. An important advantage, in this case is the absence of crystal structure that makes it possible [13–16] for them to serve as a transition layer between the substrate and the nanostructured covering, damping the difference between crystal structures of the substrate and the covering, and the difference between their thermal expansion coefficients. In many cases, these processes lead to destroying, cracking and chipping of the covering [3–5].

The results for the amorphous metal alloys of other compositions were obtained earlier [17–19] by the similar methods. This research supplements the works [17,18]. This research was performed on the material of the same system as [18], but other composition, and was supplemented by X-ray photo-electron spectroscopy (XPS). It should be noted that the results of all the research of materials with different composition correlate with each other.

2 Methods and materials

Samples of FeCr$_{15}$B$_{15}$ alloy obtained by rapid quenching (casting the melt on a cooled substrate [17–19]) were prepared to perform this research. The samples were annealed in a vacuum furnace at the different temperature for one hour. Annealing was controlled by the X-ray diffractometer. Before the crystallization, the samples showed a halo typical for the amorphous alloys and after crystallization − diffraction lines of FeCr solid solution, which testifies of the nanocrystalline phase formation [17–20].

The samples were studied by positron annihilation spectroscopy, in particular by measuring angular correlation of annihilation radiation (ACAR).

Positron annihilation spectroscopy methods are based on irradiation of the test sample by positrons and registration of annihilation photons. Measuring of the

photon emission delay concerning positron getting into the medium allows one to measure electrons' density in the annihilation area. The deviation of annihilation photons from 180° makes it possible to measure annihilated electron momentum projection on the chosen axis. It should be noted that due to its positive charge the positron is actively captured by negatively charged matrix traps, such as bulk defects as dislocations, vacancies, nanoparticles with high positron affinity, etc. It causes annihilation of more than 50% of positrons in defects even at small defects concentration. Therefore, this method is highly sensitive towards the state of the defects structure. A more detailed application of positron annihilation spectroscopy for studying defects structure is described in [19]. It was shown earlier [17,20,21] that the study of ACAR spectra makes it possible to judge about the occupancy changes in the d-shell of iron group metals. ACAR spectra were measured at the 1-D ACAR apparatus with the angular resolution of 1 mrad of the Institute for Theoretical and Experimental Physics named by A.I. Alikhanov. A detailed description of methods for data acquisition, spectra treatment and interpretation of transition metal alloys spectra is provided in [17–19].

XPS was used in this research to study energy distribution of the valence band electrons and to determine the position of the characteristic lines, which allows one to judge about the environment of the atom under study. XPS spectra were acquired by K-alpha spectrometer manufactured by Thermo fisher scientific.

Thermoelectric voltage measurement is highly sensitive towards the changes in density at Fermi level and in the population of upper electron shells [20]. Modified microhardness tester with controlled contact effort was used for this measurement. A tungsten needle was placed into the holder. The needle was heated up to the set temperature by resistive heating. The samples were studied within the temperature range from 50 to 250 °C. Contact potential difference was measured by a bridge circuit with the error of not more than ±0.01 mV. Calibration was performed for pure metals.

3 Results and discussion

Figure 1 demonstrates the dependence of the thermo electromotive force of FeCr$_{15}$B$_{15}$ amorphous metal alloy vs the annealing temperature.

Thermo electromotive force changes drastically at 400–450 °C which corresponds, in line with the results of X-ray diffractometry, to the formation start of nano-sized nucleus of FeCr solid solution [21–23].

ACAR spectra are shown in Figure 2. The spectra were approximated by the least squares method with the combination of three Gaussians and an inverted parabola considering apparatus and background resolution functions. The results are given in Table 1.

One can obtain more detailed information on the interpretation of transition metals ACAR spectra and the approximation method from the articles [24,25]. It was mentioned earlier [17–18,26–30] that the intensity of the 15–18 mrad wide Gaussian-3 correlates with the d-shell
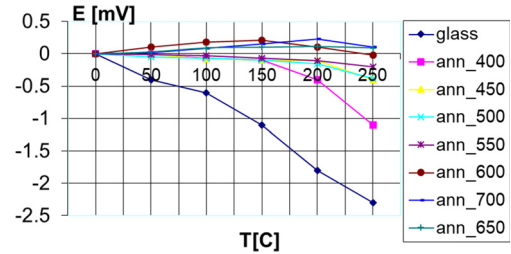

Fig. 1. Dependence of the thermo electromotive force of FeCr$_{15}$B$_{15}$ amorphous metal alloy vs the annealing temperature.

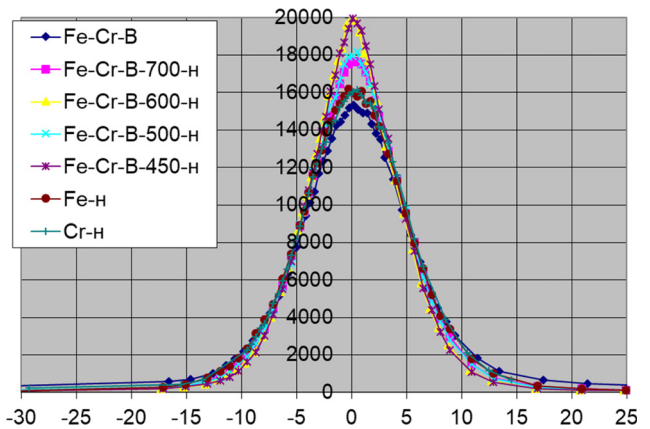**Fig. 2.** ACAR spectrum of FeCr$_{15}$B$_{15}$ alloy annealed at different temperatures as compared to pure annealed iron and chrome samples.
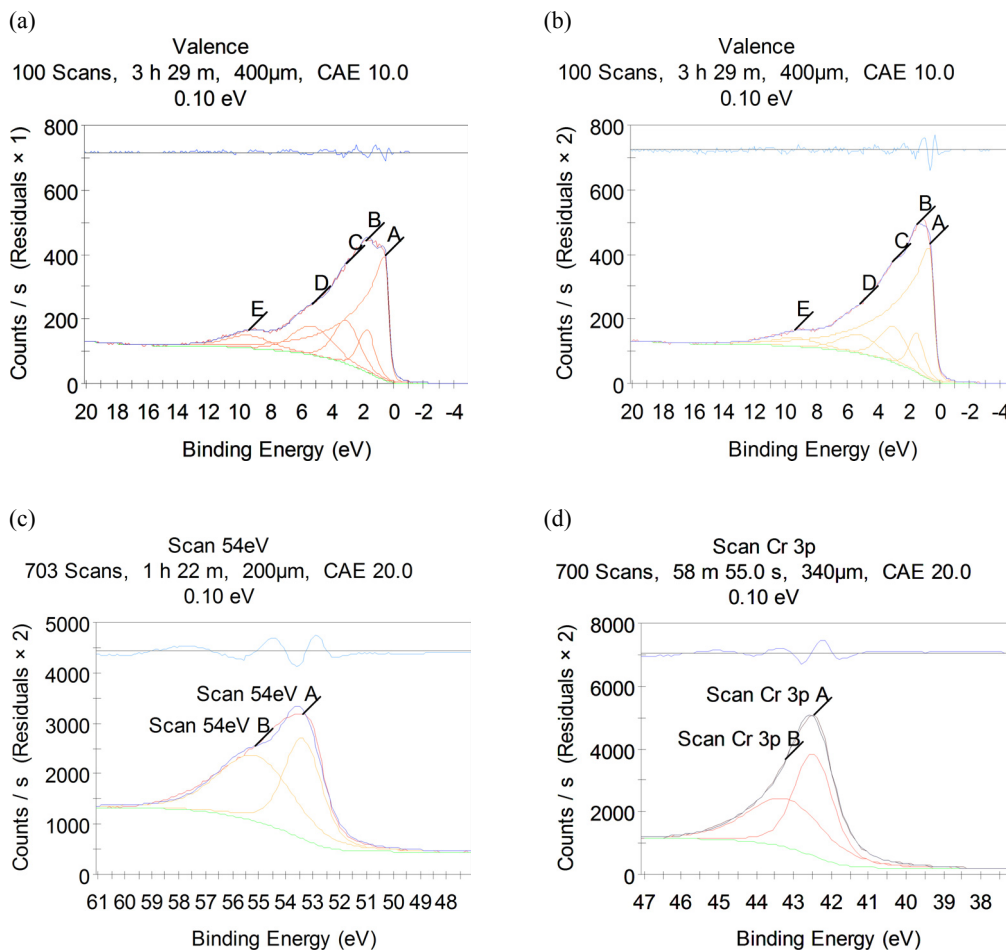
occupancy of transition group metals. The above-mentioned works contain the study of positron annihilation in transition metals. A wide Gaussian with the width of 16 ± 1.5 mrad, the intensity of which, as was shown, correlates with the d-shell occupancy, was observed in all spectra of transition metals. Parabola with the 5–6 mrad cutoff angle convolved with the 2–5 wide Gaussian is appeared in the spectra.

Considering the occupancy of this iron atom shell, which is known from the sources [31–33], it is possible to estimate the effective charge change during the FeCr$_{15}$B$_{15}$ alloy crystallization as 1 electron.

Samples of FeCr$_{15}$B$_{15}$ alloy in amorphous and crystallized states were prepared to study the the electron structure of amorphous and crystalline states using XPS. A detailed description of the samples preparation method is provided in [17]. Moreover, samples of pure iron and chrome metal were studied to obtain the basis for the valence spectra interpretation of amorphous and crystalline alloys. Amorphous samples were annealed in vacuum to obtain crystalline state. Before the study, the surface was etched by ions with the energy of 3 keV, the current being 5 μA. The etching continued until the oxygen line intensity on the panoramic spectrum fell below the level of 5%. Spectra of valence band within the range of −3–+20 eV were studied.

Table 1. Results of FeCr$_{15}$B$_{15}$ alloy PAS spectra approximation.

Sample	1 Gaussian FWHM [mrad]	Int. [%]	2 Gaussian FWHM [mrad]	Int. [%]	Parabola Cut-off angle [mrad]	Broade-ning [mrad]	3 Gaussian Int. [%]	FWHM [mrad]	Int. [%]
FeCrB amm	3.6 ± 0.8	2 ± 3	10.0 ± 0.5	68 ± 5	5.8 ± 0.4	3.5 ± 1	13.9 ± 0.8	17.7 ± 0.7	16.2 ± 1
FeCrB-450	3.1 ± 2	5 ± 2	9.8 ± 0.4	72 ± 3	6.6 ± 0.2	4.1 ± 0.4	9.7 ± 0.5	17.2 ± 0.4	12.8 ± 1.5
FeCrB-500	3.2 ± 1	3.5 ± 1.5	10.7 ± 0.7	73 ± 4	6.2 ± 0.7	2.1 ± 0.6	9.5 ± 0.7	17.8 ± 0.5	13.6 ± 1
FeCrB-600	2.9 ± 1.5	4.5 ± 2	10.1 ± 0.4	69 ± 2	5.3 ± 0.5	4.9 ± 0.9	9.5 ± 0.9	18.2 ± 0.3	11.3 ± 0.7
FeCrB-700	3.4 ± 2	3.3 ± 0.5	10.4 ± 0.9	76 ± 2	5.4 ± 0.9	4.8 ± 1.5	7.5 ± 0.7	17.9 ± 0.8	13.1 ± 1

Fig. 3. (a) XPS valence spectrum, (b) XPS valence spectrum of amorphous alloy of crystal alloy, (c) XPS Spectrum of Fe 3p level, (d) XPS Spectrum of Cr 3p of amorphous FeCrB level of amorphous FeCrB.

Initial spectra are presented in Figures 3 and 4, peak intensities are given in Tables 2 and 3. XPS spectra processing and approximation method are described in [34,35]. Valence spectrum of transition metals is defined by d-electrons, as the 4-s shell has little intensity, broad distribution and merges into the background.

The area of the amorphous sample under the valence band peaks is 14.6% higher considering the setting concerning Fe2p peak. Electron density distribution of the amorphous alloy in the valence spectrum is shifted towards the higher binding energies which correspond to bound states. The peak in the area of 9.5 eV that corresponds to the bound state of the iron-based amorphous alloy is increased. Fe3p level shift is 0.3 eV for the annealed sample, and 1.06 eV for the amorphous one. Binding energy increase of the amorphous iron Fe3s level is 0.45 eV. This value is lower for the 3p chrome peak in the FeCrB alloy and makes 0.3 eV. It demonstrates, taking into account of the research data [35–37], that the main changes during the amorphization occur in the electron structure of an iron atom.
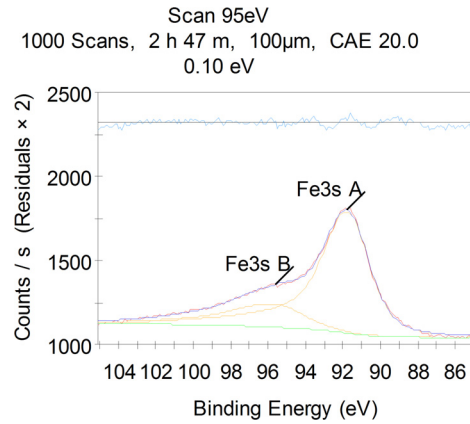
Fig. 4. Fe3s XPS spectrum of FeCr$_{15}$B$_{15}$ amorphous alloy.

Table 3. XPS peaks parameters of the FeCrB amorphous alloy.

Name	Binding energy	FWHM [eV]	Area [CPC*eV]	at. %
Fe2p	707.47	2.84	8405730.78	63.54
Cr2p	574.58	2.65	1723777.52	15.76
B1s	187.99	1.83	115632.65	20.53
Valence A	0.52	2.03	1099.47	0.09
Valence B	1.7	1.27	195.71	0.02
Valence C	3.03	1.94	308.65	0.02
Valence D	5.25	3.04	319.37	0.03
Valence E	9.42	3.5	164.49	0.01

Table 2. XPS peaks approximation parameters of the FeCrB crystalline alloy.

Name	Binding energy	FWHM [eV]	Area [CPC*eV]	at. %
Fe2p	707.32	2.8	9192468.39	65.57
Cr2p	574.58	2.56	1574852.89	14.38
B1s	188.05	1.86	112049.10	19.88
Valence A	0.6	2.30	1328.07	0.11
Valence B	1.46	1.20	170.69	0.01
Valence C	2.98	2.08	274.93	0.02
Valence D	5.19	3.04	206.48	0.02
Valence E	9.35	3.48	110.70	0.01

4 Conclusions

This research makes it possible to outline the ways for amorphous metal alloys implementation as intermediate damping layer of multilayer hard-alloy coverings. Results obtained by conjoint methods of X-ray photoelectron spectroscopy, angle correlation positron annihilation radiation and the measurement of thermo electromotive force suggest that during the thermal crystallization of an amorphous metal alloy efficient charge is redistributed between the iron atom d-shell and the conduction band. Results obtained by all the methods used in this article agree with each other well and point at the change in effective redistribution of the iron atom d-shell charge during the crystallization and the formation of the crystalline phase nano-sized nucleating seeds in the amorphous metal matrix. According to the results of the angle correlation annihilation radiation, $20 \pm 5\%$ (1 electron, according to estimates) of iron atom shell effective charge is redistributed. According to the results of the X-ray photoelectron spectroscopy such redistribution made $14.6 \pm 2\%$. These measurements in the thermo electromotive force do not allow to estimate the quantity and the direction of the effective charge redistribution; however, they agree with the aforementioned ones and make it possible to specify the process activation temperature: 400–450 °C.

References

[1] A.A. Vereschaka, A.S. Vereschaka, A.D. Batako, B.J. Mokritskii, A.Y. Aksenenko, N.N. Sitnikov, Improvement of structure and quality of nanoscale multilayered composite coatings, deposited by filtered cathodic vacuum arc deposition method, Nanomater. Nanotechnol. 7 (2017) 1–13

[2] A.A. Vereschaka, J. Prilukova, A.S. Vereshchaka, J. Bublikov, A.Y. Aksenenko, Control of temperature in cutting zone in machining of alloyed case-hardened steels by applying a ceramic tool with wear-resistant coatings, Mater. Sci. Forum 857 (2016) 199–205

[3] A.A. Vereschaka, B.Y. Mokritskii, N.N. Sitnikov, G.V. Oganyan, A.Y. Aksenenko, Study of mechanism of failure and wear of multi-layered composite nano-structured coating based on system Ti-TiN-(ZrNbTi) N deposited on carbide substrates, J. Nano Res. 45 (2017) 110–123

[4] S.N. Grigoriev, S.V. Fedorov, Tool material surface alloying by wide-aperture low-energy high-current electron beam treatment before wear-resistant coating, Mech. Ind. 16 (2015) 708

[5] I. Smurov, M. Doubenskaia, S. Grigoriev, A. Nazarov, Optical monitoring in laser cladding of Ti6Al4V, J. Therm. Spray Technol. 21 (2012) 1357–1362

[6] S.N. Grigoriev, A.S. Metel, M.A. Volosova, Yu.A. Melnik, Deposition of wear-resistant coatings using a combined source of metal atoms and fast gas molecules, Mech. Ind. 16 (2015) 705

[7] M. Lakatos-Varsanyi, R. Muranyi, F. Hajdu, R. Berenyi, L. K. Varga, Nanostructured pulsed current metal coatings of Fe and Fe-Ni for microelectronic applications, Trans. IMF 95 (2017) 6–8

[8] M.A. Volosova, S.N. Grigoriev, E.A. Ostrikov, Use of laser ablation for formation of discontinuous (discrete) wear-resistant coatings formed on solid carbide cutting tool by electron beam alloying and vacuum-arc deposition, Mech. Ind. 17 (2016) 720

[9] N. Ravi, R. Markandeya, S.V. Joshi, Fracture behaviour of nc-TiAlN/a-Si3N4 nanocomposite coating during nano-impact test, Surf. Eng. 33 (2017) 282–291

[10] G.G. Fuentes, E. Almandoz, R.J. Rodriguez, H. Dong, Y. Qin, S. Mato, F.J. Perez-Trujillo, Vapour deposition technologies for the fabrication of hot-forming tools: a review, Manuf. Rev. 1 (2014) 20

[11] E. Axinte, A. Bofu, Y. Wang, A.M. Abdul-Rani, A.A. Abdu Aliyu, An overview on the conventional and nonconventional methods for manufacturing the metallic glasses, MATEC Web Conf. 112 (2017) 03003

[12] M.M. Stebulyanin, A.A. Gurkina, A.A. Shein, N.Y. Cherkasova, Measuring adhesive bond strength and microhardness of multilayer composite wear-resistant coating, Mech. Ind. 17 (2016) 712

[13] V.V. Kuzin, M.Y. Fedorov, M.A. Volosova, Nitride ceramic surface layer stressed state transformation with a change in TiC-coating thickness. Stress − distributed force load version, Refract. Ind. Ceram. 57 (2017) 551–556

[14] X. Wei, P. Zhang, D. Wei, H. Zhao, C. Wang, T. Liskiewicz, Mechanical and tribological properties of Cr-Nb double-glow plasma coatings deposited on Ti-Al alloy, Tribol. Mater. Surf. Interfaces 11 (2017) 98–106

[15] K. Bobzin, T. Brogelmann, N.C. Kruppe, M. Arghavani. J. Mayer, T.E. Weirich, Plastic deformation behavior of nanostructured CrN/AlN multilayer coatings deposited by hybrid dcMS/HPPMS, Surf. Coat. Technol. 332 (2017) 253–261

[16] M.M. Quazi, M. Ishak, A. Arslan, M.N. Bashir, I. Ali, Scratch adhesion and wear failure characteristics of PVD multilayer CrTi/CrTiN thin film ceramic coating deposited on AA7075-T6 aerospace alloy, J. Adhes. Sci. Technol. (2017) 1–7

[17] V.I. Grafutin, Y.V. Funtikov, N.O. Khmelevsky, Electronic properties of the amorphous FeCuNbSiB alloy, Phys. Solid State 54 (2012) 28–30

[18] Y.V. Funtikov, O.V. Prokopjev, N.O. Khmelevsky, O.V. Ilyukhina, V.I. Grafutin, V.S. Khmelevskaya, K.A. Gorchakov, Electron transport properties of iron-based amorphous alloys under crystallization, J. Surf. Investig. X-ray, Synchrotron Neutron Tech. 4 (2010) 609–613

[19] V.I. Grafutin, Y.V. Funtikov, N.O. Khmelevsky, Positron annihilation spectroscopy of iron group metals, High Energy Chem. 46 (2012) 71–72

[20] Z. Tang, T. Chiba, Y. Nagai, K. Inoue, T. Toyama, M. Hasegawa, Positron annihilation study for enhanced nitrogen-vacancy center formation in diamond by electron irradiation at 77 K, Appl. Phys. Lett. 104 (2014) 172101

[21] T. Suzudo, Y. Nagai, D. Schwenc, A. Caro, Hardening in thermally-aged Fe-Cr binary alloys: Statistical parameters of atomistic configuration, Acta Mater. 89 (2015) 116–122

[22] A.I. Salimon, A.P. Shevchukov, A.A. Stepashkin, V.V. Tcherdyntsev, L.K. Olifirov, S.D. Kaloshkin, Mechanical alloying as a solid state route for fabrication of Al-Cu-M (=Fe, Cr) quasicrystalline phases, J. Alloys Compd. 707 (2017) 315–320

[23] Y. Geng, T. Ablekim, M.A. Koten, M. Weber, K. Lynn, J.E. Shield, Defect generation and analysis in mechanically alloyed stoichiometric Fe-Ni alloys, J. Alloys Compd. 633 (2015) 250–255

[24] L.U. Dubov, Y.V. Shtotsky, Y.A. Akmalova, Y.V. Funtikov, V.V. Palacheva, A.I. Bazlov, I.S. Golovin, Ordering processes in Fe-Ga alloys studied by positron annihilation lifetime spectroscopy, Mater. lett. 171 (2016) 46–49

[25] S.V. Stepanov, V.M. Byakov, D.S. Zvezhinskiy, G. Duplatre, L.Y. Dubov, P.S. Stepanov, Y.D. Perfiliev, L.A. Kulikov, Premelting as studied by positron annihilation and emission Mossbauer spectroscopies, J. Phys. Conf. Ser. 674 (2016) 012018

[26] J. Jiang, Y.C. Wu, X.B. Liu, R.S. Wang, Y. Nagai, K. Inoue, Y. Shimizu, T. Toyama, Microstructural evolution of RPV steels under proton and ion irradiation studied by positron annihilation spectroscopy, J. Nucl. Mater. 458 (2015) 326–334

[27] T.A. Sviridova, A.P. Shevchukov, E.V. Shelekhov, D.L. Diakonov, V.V. Tcherdyntsev, S.D. Kaloshkin, The quasicrystalline phase formation in Al-Cu-Cr alloys produced by mechanical alloying, J. Alloys Compd. 509 (2011) 299–303

[28] Y. Matsukawa, T. Takeuchi, Y. Kakubo, T. Suzudo, H. Watanabe, H. Abe, T. Toyama, Y. Nagai, The two-step nucleation of G-phase in ferrite, Acta Mater. 116 (2016) 104–114

[29] V.V. Tcherdyntsev, T.A. Sviridova, A.P. Shevchukov, S.D. Kaloshkin, Quasicrystals formation in ball-milled Al-Cu-Cr powders, J. Phys. Conf. Ser. 144 (2009) 012–024

[30] G. Bonny, N. Castin, C. Domain, P. Olsson, B. Verreyken, M.I. Pascuet, D. Terentyev, Density functional theory-based cluster expansion to simulate thermal annealing in FeCrW alloys, Philos. Mag. 97 (2017) 299–317

[31] P. Asoka-Kumar, M. Alatalo, V.J. Ghosh, A.C. Kruseman, B. Nielsen, K.G. Lynn, Increased elemental specificity of positron annihilation spectra, Phys. Rev. Lett. 77 (1996) 2097–2100

[32] O. Prytz, J. Tafto, C.C. Ahn, B. Fultz, Transition metal d-band occupancy in skutterudites studied by electron energy-loss spectroscopy, Phys. Rev. B 75 (2007) 125109

[33] N.V. Korobova, A.Y. Aksenenko, O.S. Bashevskaya, A.A. Nikitin, Study of the effect of modes of electroerosion treatment on the microstructure and accuracy of precision sizes of small parts, Met. Sci. Heat Treat. 57 (2016) 585–588

[34] A.A. Volykhov, J. Sanchez-Barriga, A.P. Sirotina, V.S. Neudachina, A.S. Frolov, E.A. Gerber, E.Y. Kataev, B. Senkovsky, N.O. Khmelevsky, A.Y. Aksenenko, N.V. Korobova, A. Knop-Gericke, O. Rader, L.V. Yashina, Rapid surface oxidation of Sb2Te3 as indication for a universal trend in the chemical reactivity of tetradymite topological insulators, Chem. Mater. 28 (2016) 8916–892

[35] S.A. Vladimirova, M.N. Rumyantseva, D.G. Filatova, A.S. Chizhov, N.O. Khmelevsky, E.A. Konstantinova, V.F. Kozlovsky, A.V. Marchevsky, O.M. Karakulina, J. Hadermann, A.M. Gaskov, Cobalt location in p-CoOx/n-SnO2 nanocomposites: correlation with gas sensor performances, J. Alloys Compd. 721 (2017) 249–260

[36] P. Tsai, K. Flores, High-throughput discovery and characterization of multicomponent bulk metallic glass alloys, Acta Mater. 120 (2016) 426–434

[37] Y. Geng, T. Ablekim, P. Mukherjee, M. Weber, J.E. Shield, High-energy mechanical milling-induced crystallization in Fe32Ni52Zr3B13, J. Non-Cryst. Solids 404 (2014) 140–144